INTERNATIONAL JOURNAL FOR NUMERICAL AND ANALYTICAL METHODS IN GEOMECHANICS
Int. J. Numer. Anal. Meth. Geomech. 2007; **31**:1375–1399
Published online 29 January 2007 in Wiley InterScience (www.interscience.wiley.com). DOI: 10.1002/nag.601

An operator-split ALE model for large deformation analysis of geomaterials

Y. Di[1], J. Yang[2,*,†] and T. Sato[3,4]

[1]*LTCS and Department of Mechanics and Engineering Science, Peking University, China*
[2]*Department of Civil Engineering, The University of Hong Kong, China*
[3]*Disaster Prevention Research Institute, Kyoto University, Japan*
[4]*Faculty of Science and Engineering, Waseda University, Japan*

SUMMARY

Analysis of large deformation of geomaterials subjected to time-varying load poses a very difficult problem for the geotechnical profession. Conventional finite element schemes using the updated Lagrangian formulation may suffer from serious numerical difficulties when the deformation of geomaterials is significantly large such that the discretized elements are severely distorted. In this paper, an operator-split arbitrary Lagrangian–Eulerian (ALE) finite element model is proposed for large deformation analysis of a soil mass subjected to either static or dynamic loading, where the soil is modelled as a saturated porous material with solid–fluid coupling and strong material non-linearity. Each time step of the operator-split ALE algorithm consists of a Lagrangian step and an Eulerian step. In the Lagrangian step, the equilibrium equation and continuity equation of the saturated soil are solved by the updated Lagrangian method. In the Eulerian step, mesh smoothing is performed for the deformed body and the state variables obtained in the updated Lagrangian step are then transferred to the new mesh system. The accuracy and efficiency of the proposed ALE method are verified by comparison of its results with the results produced by an analytical solution for one-dimensional finite elastic consolidation of a soil column and with the results from the small strain finite element analysis and the updated Lagrangian analysis. Its performance is further illustrated by simulation of a complex problem involving the transient response of an embankment subjected to earthquake loading. Copyright © 2007 John Wiley & Sons, Ltd.

Received 2 February 2006; Revised 19 November 2006; Accepted 7 December 2006

KEY WORDS: finite strain; ALE model; saturated soil; porous media; non-linearity; dynamics

*Correspondence to: J. Yang, Department of Civil Engineering, The University of Hong Kong, Pokfulam, Hong Kong, China.
†E-mail: junyang@hku.hk

Contract/grant sponsor: Research Grants Council of Hong Kong; contract/grant number: HKU7191/05E.

1. INTRODUCTION

The finite element formulations for quantitative study of the static and/or dynamic behaviour of saturated soils were established decades ago [1–5]. In general, the formulations are based on the effective stress principle, transient pore fluid movement, generalized material stiffness and infinitesimal strain theory. It is now widely accepted that many problems in geotechnical engineering practice involve large deformations for which the infinitesimal strain theory may not be applicable. Typical large deformation problems include failure of embankments due to soil liquefaction, slope instability and landslide, penetration of piles and penetrometers. There is currently an increasing concern over the large deformation effect in geotechnical analyses.

Several numerical schemes have been developed for large deformation analysis in geomechanics [6–10]. Most of them involve the Lagrangian finite element formulation in which relevant quantities are described with respect to the initial co-ordinate (total Lagrangian) or fixed to the geometry at the beginning of the time step and moved with the material (updated Lagrangian). When the finite element discretization is implemented, the configuration of the material body is covered with a finite element mesh. Nodes are associated with the same material particles throughout the deformation process of the body, and the mesh is then deformed along with the body. The Lagrangian formulation is particularly suited for problems concerning path-dependent material with free surface conditions. However, in the case of very large deformation where severe mesh distortion and element entanglement occur, the Lagrangian reference state may not be viable for subsequent step analysis, as manifested by instability or interruption of the numerical computation.

There is another method for large deformation analysis, known as the Eulerian formulation. In this method, the finite element mesh can be selected and fixed in space while the material flows through the mesh. It is difficult, however, to convert material particles on a fixed mesh and, consequently, not easy to present the free boundary condition and simulate the deformation history of the material.

An arbitrary Lagrangian–Eulerian (ALE) finite element model is presented in this paper to combine the advantages of the two formulations described above while avoiding their drawbacks. In the ALE analysis, a reference computational domain is introduced and the finite element mesh is neither attached to the material nor fixed in space. Motion of the mesh is independent of that of the material. As a result, the ALE formulation can handle path-dependent material behaviour and free surface conditions while maintaining the mesh fineness. The ALE finite element method was first proposed for solving problems of fluid mechanics, and then used to solve problems of solid mechanics [11–15]. To the authors' best knowledge there is no ALE finite element model for large deformation analysis of saturated soils that exhibit strong material non-linearity and complex solid-fluid interaction.

The ALE procedures can be divided into coupled and operator-split ALE formulations. In the first, fully coupled Lagrangian–Eulerian equations involving both material and mesh velocities are solved [15, 16]. In the second formulation, which is more convenient and efficient for computation, an operator-split scheme is used and the coupled Lagrangian–Eulerian equations are split and solved separately [17]. In this paper, the operator-split ALE formulation is established for large deformation analysis of a saturated soil mass subjected to either static or dynamic loading. The saturated soil is modelled as a two-phase mixture composed of the deforming solid skeleton and the saturating pore fluid, and the material non-linearity exhibited by most soils is incorporated. The performance of the proposed ALE model is evaluated and demonstrated in detail using two examples.

DOI: 10.1002/nag

2. GOVERNING EQUATIONS

The saturated soil is considered as a two-phase material with a soil skeleton and a pore fluid phase. The governing equations for the saturated soil are briefly presented in this section.

2.1. Equilibrium equation

For a mixture of the two-phase material, the effective and partial stresses are defined as

$$\sigma'_{ij} = \sigma_{ij} + p\delta_{ij} \tag{1}$$

$$\sigma_{ij} = \sigma^{\mathrm{s}}_{ij} + \sigma^{\mathrm{f}}_{ij} \tag{2}$$

$$\sigma^{\mathrm{s}}_{ij} = \sigma'_{ij} - (1-n)p\delta_{ij} \tag{3}$$

$$\sigma^{\mathrm{f}}_{ij} = -np\delta_{ij} \tag{4}$$

where σ_{ij} is the Cauchy total stress in the combined solid and fluid mixture, σ'_{ij} the effective stress, p the pore water pressure (taken positive when compressive), σ^{s}_{ij} the partial stress in the solid phase, σ^{f}_{ij} the partial stress in the fluid phase, n the porosity, and δ_{ij} the Kronecker delta.

Each of the components of the two-phase medium is regarded as a continuum and follows its own motion equations. The equation of motion for the solid phase is

$$\frac{\partial \sigma^{\mathrm{s}}_{ij}}{\partial x_j} + (1-n)\rho^{\mathrm{s}} b_i - (1-n)\rho^{\mathrm{s}}\dot{v}_i - R_i = 0 \tag{5}$$

$$R_i = -\frac{n\gamma^{\mathrm{f}}}{k}\dot{w}_i \tag{6}$$

where v_i is the velocity of the soil skeleton, v^{f}_i the velocity of the fluid phase, b_i the body force acceleration, ρ^{s} the density of soil particles, k the Darcy permeability coefficient, γ^{f} the unit weight of the fluid phase, R_i the viscous drag force acting on the fluid phase caused by the soil skeleton, and w_i describes the fluid displacement relative to the skeleton of soils.

$$\dot{w}_i = n(v^{\mathrm{f}}_i - v_i) \tag{7}$$

For the pore fluid, its equation of motion can be written as

$$\frac{\partial \sigma^{\mathrm{f}}_{ij}}{\partial x_j} + n\rho^{\mathrm{f}} b_i - n\rho^{\mathrm{f}}\dot{v}^{\mathrm{f}}_i + R_i = 0 \tag{8}$$

From Equations (5) and (8), and adopting the u–p formulation [4], the equilibrium equation of motion for the total mixture of soil skeleton and fluid phase is simplified as

$$\frac{\partial \sigma_{ij}}{\partial x_j} + \rho b_i - \rho\ddot{u}_i = 0 \tag{9}$$

where u_i is the displacement of the solid skeleton and ρ the apparent density of saturated soils.

DOI: 10.1002/nag

2.2. Continuity equation

According to the law of mass conservation, the local form for soil skeleton is

$$\frac{\partial(\rho^{\mathrm{s}}(1-n))}{\partial t}+\frac{\partial(\rho^{\mathrm{s}}(1-n)v_i)}{\partial x_i}=0 \tag{10}$$

Similarly, for the fluid it is

$$\frac{\partial(n\rho^{\mathrm{f}})}{\partial t}+\frac{\partial(n\rho^{\mathrm{f}}v_i^{\mathrm{f}})}{\partial x_i}=0 \tag{11}$$

Combining Equations (10) and (11) gives

$$\frac{\partial \dot{w}_i}{\partial x_i}+d_{ii}+n\frac{\dot{\rho}^{\mathrm{f}}}{\rho^{\mathrm{f}}}+(1-n)\frac{\dot{\rho}^{\mathrm{s}}}{\rho^{\mathrm{s}}}=0 \tag{12}$$

where d_{ij} is the symmetric rate of the deformation tensor.

The soil particles are assumed as incompressible and, therefore, ρ^{s} is constant and $\dot{\rho}^{\mathrm{s}}$ is zero. The material derivative, $\dot{\rho}^{\mathrm{f}}$, of the fluid phase density is related to the material derivative, $\dot{p}$, of the pore pressure by

$$\dot{\rho}^{\mathrm{f}}=\frac{\dot{p}}{K^{\mathrm{f}}}\rho^{\mathrm{f}} \tag{13}$$

where K^{f} is the bulk modulus of the fluid phase.

Substituting Equation (13) in Equation (12) gives

$$\frac{\partial \dot{w}_i}{\partial x_i}+d_{ii}+\frac{n}{K^{\mathrm{f}}}\dot{p}=0 \tag{14}$$

The distribution of the porosity is assumed to be smooth enough in the soil, then Equation (14) is simplified as [18]

$$-\frac{k}{g}\dot{d}_{ii}-\frac{k}{\gamma^{\mathrm{f}}}\left(\frac{\partial^2 p_{\mathrm{E}}}{\partial^2 x_i}\right)_i+d_{ii}+\frac{n}{K^{\mathrm{f}}}\dot{p}_{\mathrm{E}}=0 \tag{15}$$

where p_{E} is excess pore pressure and g the gravitational constant.

Equations (9) and (15) define a coupled form of the governing equations for a saturated soil.

2.3. Constitutive equation

To describe the non-linear behaviour of saturated soil, the elasto-plastic constitutive model proposed by Oka *et al*. [19] is adopted. This model is based on the non-linear kinematic hardening and non-associated flow rules. The accumulations of strain and pore water pressure during cyclic loading are taken into account. The capability of this constitutive model has been examined by comparisons between experimental results and numerical simulations. Details of this constitutive model and parameter calibration are described in [19, 20].

Because large deformation is considered here, an objective measure of stress should be adopted. Jaumann stress rate is objective but not exact in the case of both large deformations and large

DOI: 10.1002/nag

material rotations. However, it is accurate enough for small strains and large material rotations, as considered by Hughes *et al*. [21]. An accurate large deformation analysis can thus be developed adopting Jaumann stress rate in an updated Lagrangian approach with small strain increments in each time step of the analysis. A general linear relationship between the objective stress rate and the deformation rate can be written in the form

$$\dot{\sigma}_{ij}^{\mathrm{J}} = D_{ijkl} d_{kl} - \dot{p}\delta_{ij} \tag{16}$$

where $\dot{\sigma}_{ij}^{\mathrm{J}}$ is Jaumann stress rate, $\dot{p}$ the rate of pore pressure and D_{ijkl} the elasto-plastic tensor of the constitutive model.

The rate of stress can be obtained as

$$\dot{\sigma}_{ij} = \dot{\sigma}_{ij}^{\mathrm{J}} + \sigma_{ik}\omega_{jk} + \sigma_{jk}\omega_{ik} = D_{ijkl} d_{kl} - \dot{p}\delta_{ij} + \sigma_{ik}\omega_{jk} + \sigma_{jk}\omega_{ik} \tag{17}$$

where $\dot{\sigma}_{ij}$ is the rate of stress and ω_{ij} the skew symmetric spin tensor.

3. OPERATOR-SPLIT ALE MODEL

3.1. Fundamentals of ALE

In large deformation analysis, the state variables (motion, deformation and strain etc.) of a continuum can be described in three different ways. In Lagrangian description, the material particles are labelled by the co-ordinates, X_i, at their initial positions and state variables are functions of the material co-ordinates. In Eulerian description, the current positions of these particles are located by the spatial co-ordinates, x_i, and state variables are a function of the current spatial co-ordinates. In the ALE description, a referential domain, which is composed of the co-ordinates χ_i of grid points of mesh, is employed to describe the state variables. Define that u_i and v_i are the displacement and velocity of the soil skeleton at time t, $\hat{u}_i$ and $\hat{v}_i$ are the displacement and velocity of the mesh grid on the material at time t. The soil skeleton displacement u_i and the mesh grid displacement $\hat{u}_i$ on the material have the following forms:

$$u_i(X_j, t) = x_i(X_j, t) - x_i(X_j, 0) \quad (i, j = 1, 2, 3) \tag{18}$$

$$\hat{u}_i(\chi_j, t) = x_i(\chi_j, t) - x_i(\chi_j, 0) \quad (i, j = 1, 2, 3) \tag{19}$$

The material velocity v_i and the mesh velocity $\hat{v}_i$ can be obtained by differentiating the equations of material motion and mesh motion with respect to time while keeping the particle X_j or the mesh grid point χ_j fixed

$$v_i = \frac{\mathrm{d}u_i}{\mathrm{d}t} = \left.\frac{\partial x_i(X_j, t)}{\partial t}\right|_{X_j} \tag{20}$$

$$\hat{v}_i = \frac{\mathrm{d}\hat{u}_i}{\mathrm{d}t} = \left.\frac{\partial x_i(\chi_j, t)}{\partial t}\right|_{\chi_j} \tag{21}$$

DOI: 10.1002/nag

Convective velocity c_i should be introduced to map the convective effects between the material and grid as

$$c_i = v_i - \hat{v}_i \tag{22}$$

Although the mesh and material motion are independent of each other, a one-to-one mapping between material and computational referential domains should be guaranteed. The boundaries of the two domains should coincide, requiring that

$$(v_i - \hat{v}_i)n_i = 0 \text{ on the boundary} \tag{23}$$

where n_i is the normal vector at any point on the boundary.

Assuming that function f is defined by the spatial co-ordinate x_i, and that f can be stress, strain, or any history variable, then one may have

$$f(x_i, t) = f(x_i(X_j, t), t) = \tilde{f}(X_j, t) = f(x_i(\chi_j, t), t) = \hat{f}(\chi_j, t) \quad (i, j = 1, 2, 3) \tag{24}$$

The material and ALE computational referential time derivatives of function f are

$$\dot{f} = \left.\frac{\partial \tilde{f}}{\partial t}\right|_{X_i} = \left.\frac{\partial f}{\partial t}\right|_{x_i} + v_j \frac{\partial f}{\partial x_j} \tag{25}$$

$$f' = \left.\frac{\partial \hat{f}}{\partial t}\right|_{\chi_i} = \left.\frac{\partial f}{\partial t}\right|_{x_i} + \hat{v}_j \frac{\partial f}{\partial x_j} \tag{26}$$

From Equations (25) and (26), the referential derivative f' is related to the material derivative $\dot{f}$ by

$$\dot{f} = f' + c_j \frac{\partial f}{\partial x_j} \tag{27}$$

Substituting Equation (27) into the governing Equations (9) and (15), an coupled ALE formulation for the saturated medium can be derived [22].

Several methods have been proposed to solve the fully coupled equations [23, 24], but the procedures involved are very complicated and the computation is costly. An alternative method, referred to as the operator-split technique [17], is adopted in this study.

In the operator-split ALE method, each time step of analysis is divided into two parts: a Lagrangian step and an Eulerian step, which are solved separately. In the Lagrangian step, the finite element mesh follows the material deformation, and a pure updated Lagrangian procedure is done. Then mesh smoothing is performed and the computational reference system (mesh) is changed as required. Finally the state variables are transferred from the Lagrangian mesh to the new reference mesh to complete the Eulerian step. The advantage of the operator-split method over the fully coupled approach is that it breaks very complicated equations into simpler ones that can be solved more easily.

3.2. Updated Lagrangian step

It is assumed that the reference system (mesh) follows the material particle flow during this step. Consequently, this step is a classical Lagrangian formulation calculation.

DOI: 10.1002/nag

In the updated Lagrangian (UL) method, the relevant quantities, such as stress and strain, are correlated with the reference configuration at time t. The governing equations of the saturated soil are satisfied at the end of each time step, $t+\Delta t$. The weak formulation of equilibrium Equation (9) and continuity Equation (15) are

$$\int_{{}^tV} \rho\, {}^{t+\Delta t}\ddot{u}_i \delta v_i \,\mathrm{d}\,{}^tV + \int_{{}^tV} \left(\int_t^{t+\Delta t} \dot{S}_{ij}\,\mathrm{d}t \right) \delta \dot{E}_{ij}\,\mathrm{d}\,{}^tV + \int_{{}^tV} {}^t\sigma_{ij}\delta\dot{E}_{ij}\,\mathrm{d}\,{}^tV$$
$$= \int_{{}^{t+\Delta t}A} {}^{t+\Delta t}t_i \delta v_i \,\mathrm{d}\,{}^{t+\Delta t}A + \int_{{}^{t+\Delta t}V} \rho\, {}^{t+\Delta t}b_i \delta v_i \,\mathrm{d}\,{}^{t+\Delta t}V \tag{28}$$

$$\int_{{}^tV} \rho^{\mathrm{f}}\, {}^{t+\Delta t}\dot{d}_{ii}\,\mathrm{d}\,{}^tV - \int_{{}^tV} \frac{\gamma^{\mathrm{f}}}{k}\, {}^{t+\Delta t}d_{ii}\,\mathrm{d}\,{}^tV + \int_{{}^tV} \left(\frac{\partial^2 ({}^{t+\Delta t}p_{\mathrm{E}})}{\partial x_i^2} \right)_i \mathrm{d}\,{}^tV$$
$$- \int_{{}^tV} \frac{n\gamma^{\mathrm{f}}}{kK^{\mathrm{f}}}\, {}^{t+\Delta t}\dot{p}_{\mathrm{E}}\,\mathrm{d}\,{}^tV = 0 \tag{29}$$

where ${}^tV$ is element volume bounded by a surface ${}^tA$, ${}^t\sigma_{ij}$ is the Cauchy stress tensor at time t, Δt is the increment of the time step, ${}^{t+\Delta t}\ddot{u}_i$ the acceleration of the solid skeleton at time $t+\Delta t$, $\dot{S}_{ij}$ the second Piola–Kirchhoff stress rate, $\dot{E}_{ij}$ the Lagrangian strain rate, ${}^{t+\Delta t}p_{\mathrm{E}}$ the excess pore pressure at time $t+\Delta t$, ${}^{t+\Delta t}b_i$ is the force acceleration per unit volume and ${}^{t+\Delta t}t_i$ the traction.

By use of the finite element and finite difference hybrid method [10, 18] and by introducing Rayleigh damping, the numerical formulations of the coupled Equations (28) and (29) are obtained as

$$[M]\{{}^{t+\Delta t}\ddot{U}\} + [C]\{{}^{t+\Delta t}\dot{U}\} + [K]\{\Delta U\} + [K_{\mathrm{V}}]\{{}^{t+\Delta t}p_{\mathrm{E}}\} = \{F\} \tag{30}$$

$$\rho^{\mathrm{f}}[K_{\mathrm{V}}]^{\mathrm{T}}\{{}^{t+\Delta t}\ddot{U}\} - \frac{\gamma^{\mathrm{f}}}{k}[K_{\mathrm{V}}]^{\mathrm{T}}\{{}^{t+\Delta t}\dot{U}\} + [a]\{{}^{t+\Delta t}p_{\mathrm{E}}\} - [A]\{{}^{t+\Delta t}\dot{p}_{\mathrm{E}}\} = 0 \tag{31}$$

where $\{{}^{t+\Delta t}U\}$ is the nodal displacement vector, $\{{}^{t+\Delta t}p_{\mathrm{E}}\}$ the excess pore pressure vector of elements, $[M]$ the mass matrix, $[K]$ the total stiffness matrix including a material stiffness part and a geometrical one, $[C]$ the damping matrix, $[K_{\mathrm{V}}]$ makes up the coupling matrix, $\{F\}$ is the total load vector, and $[a]$ and $[A]$ are two matrices involving excess pore pressure and its rate.

For the excess pore pressure, the following equation is obtained with the backward finite difference method:

$$\{{}^{t+\Delta t}\dot{p}_{\mathrm{E}}\} = \frac{\{{}^{t+\Delta t}p_{\mathrm{E}}\} - \{{}^tp_{\mathrm{E}}\}}{\Delta t} \tag{32}$$

Using Newmark's β method, the nodal displacement and velocity at time $t+\Delta t$ are expressed as

$$\{{}^{t+\Delta t}U\} = \{{}^tU\} + \{\Delta U\} = \Delta t\{{}^t\dot{U}\} + \frac{(\Delta t)^2}{2}\{{}^t\ddot{U}\} + \beta(\Delta t)^2(\{{}^{t+\Delta t}\ddot{U}\} - \{{}^t\ddot{U}\}) \tag{33}$$

$$\{{}^{t+\Delta t}\dot{U}\} = \{{}^t\dot{U}\} + \Delta t\{{}^t\ddot{U}\} + \gamma\Delta t(\{{}^{t+\Delta t}\ddot{U}\} - \{{}^t\ddot{U}\}) \tag{34}$$

where β and γ are parameters of Newmark's β method.

DOI: 10.1002/nag

Substitution of Equations (32)–(34) into Equations (30) and (31) results in the coupled equation in the following matrix form:

$$\begin{bmatrix} ([M]+\gamma\Delta t[C]+\beta(\Delta t)^2[K]) & [K_{\mathrm{V}}] \\ [K_{\mathrm{V}}]^{\mathrm{T}} & \dfrac{\Delta t[a]-[A]}{\Delta t\alpha\gamma^{\mathrm{f}}} \end{bmatrix} \begin{Bmatrix} \{^{t+\Delta t}\ddot{U}\} \\ \{^{t+\Delta t}p_{\mathrm{E}}\} \end{Bmatrix}$$

$$= \begin{Bmatrix} \left(\{F\}-[C](\{^t\dot{U}\}+(1-\gamma)\Delta t\{^t\ddot{U}\})-[K]\left(\Delta t\{^t\dot{U}\}+\left(\frac{1}{2}-\beta\right)(\Delta t)^2\{^t\ddot{U}\}\right)\right) \\ \dfrac{[K_{\mathrm{V}}]^{\mathrm{T}}}{\alpha k}(\{^t\dot{U}\}+(1-\gamma)\Delta t\{^t\ddot{U}\})+\dfrac{[A]}{\Delta t\alpha\gamma^{\mathrm{f}}}\{^t p_{\mathrm{E}}\} \end{Bmatrix} \tag{35}$$

where $\alpha=\left(\dfrac{1}{g}-\dfrac{\gamma\Delta t}{k}\right)$.

3.3. Mesh smoothing

After the updated Lagrangian step is completed, the solution freezes, whereas the finite element mesh (reference system) is moved as desired. The element nodal pattern is defined by creating a new mesh for the deformed body. Various methods such as h-adaptivity, p-adaptivity and r-adaptivity techniques have been proposed for remeshing of the structure. The h-adaptivity method changes the mesh connectivity through addition of elements. The p-adaptivity method enhances the polynomial interpolation space in high strain location regions. The r-adaptivity method refines the mesh by relocation of nodes. In order to avoid complicated computation, the mesh-smoothing scheme in this paper moves nodes as in the r-adaptivity method. Compared to the conventional mesh refinement that requires significant computational efforts, this smoothing scheme is explicit and computationally cheap.

In doing the mesh smoothing, first, element distortion is detected and the nodes associated with the distorted elements are moved. The distortion factor proposed by Zavattieri *et al*. [25] is adopted to measure the element quality

$$Q_k = C_{\mathrm{d}}\frac{V_k}{P_k^d} \tag{36}$$

where Q_k is the quality factor of element k, V_k represents its volume, and P_k its perimeter; $d=2$ for 2D or $d=3$ for 3D problem, and C_d is a constant (equals 20.78 for a triangular element and 16.00 for a quadrilateral).

When an element is being distorted, its value Q_k decreases towards zero. The quality factor of global mesh is given by

$$Q = \min\{Q_k\} \tag{37}$$

Secondly, relocation of all selected nodes is decided. For an element i surrounding an interior node k (see Figure 1), the co-ordinates of gravity centre of the element are

$$\mathbf{x}_i^{\mathrm{C}} = \frac{1}{n_{\mathrm{n}}}\left(\sum_{j=1}^{n_{\mathrm{n}}^*}\mathbf{x}_j^{\mathrm{M}} + \sum_{j=n_{\mathrm{n}}^*}^{n_{\mathrm{n}}}\mathbf{x}_j^{\mathrm{G}}\right) \tag{38}$$

DOI: 10.1002/nag

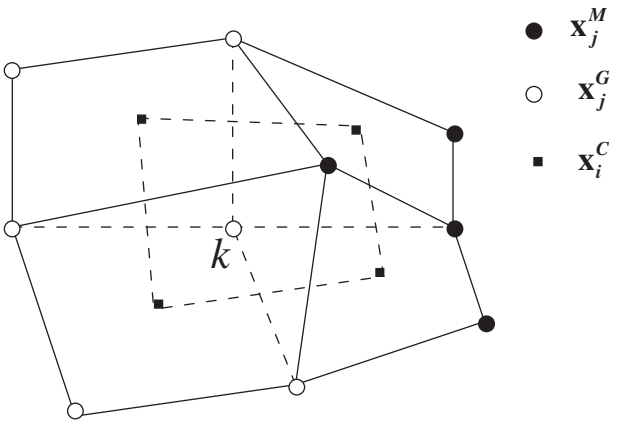

Figure 1. Relocation of an interior node.

where n_n is the number of nodes in the element i, n_n^* the number of un-relocated nodes in the element i, $\mathbf{x}_j^\mathrm{M}$ the nodal co-ordinates, $\mathbf{x}_j^\mathrm{G}$ the relocated co-ordinates. The new position of the node k can be calculated as

$$\mathbf{x}_k^\mathrm{G} = \frac{1}{W_\mathrm{T}} \left(\sum_{i=1}^{n_\mathrm{e}} \mathbf{x}_i^\mathrm{C} W_i \right) \tag{39}$$

where W_i is the weight factor of element i, n_e the number of elements surrounding the node k, $W_\mathrm{T} = \sum_{i=1}^{n_\mathrm{e}} W_i$.

Although the mesh and material motions are independent of each other, the boundaries of the two domains should coincide. To ensure this the relocation of all selected nodes on the boundaries should satisfy Equation (23). As shown in Figure 2, $\mathbf{x}_1^\mathrm{M}$, $\mathbf{x}_2^\mathrm{M}$ and $\mathbf{x}_3^\mathrm{M}$ are three nodes on the boundary. To relocate the node $\mathbf{x}_2^\mathrm{M}$, a quadratic curve defined by the three nodes is used [26]. The new position of the node $\mathbf{x}_2^\mathrm{M}$ is determined by

$$\mathbf{x}_2^\mathrm{G} = \sum_{\alpha=1}^{3} \varphi_\alpha \mathbf{x}_\alpha^\mathrm{M} \tag{40}$$

where $\varphi_1 = \frac{1}{2}\xi(\xi - 1)$, $\varphi_2 = (1 - \xi)(1 + \xi)$, $\varphi_3 = \frac{1}{2}\xi(\xi + 1)$, $\xi = (D_{23} - D_{21})/(D_{21} + D_{23})$, $D_{ij} = \sqrt{\sum_{k=1}^{3} (x_{ik}^\mathrm{M} - x_{jk}^\mathrm{M})^2}$.

3.4. Transferring of state variables

After smoothing the mesh, a new mesh pattern is created and used as the reference configuration. The state variables (stress, strain, etc.) obtained in the updated Lagrangian step are then transferred onto the new mesh from the old one. The aim of this step is to solve Equation (27). In this paper the Godunov method [27, 28] is used to transfer the state variables.

DOI: 10.1002/nag

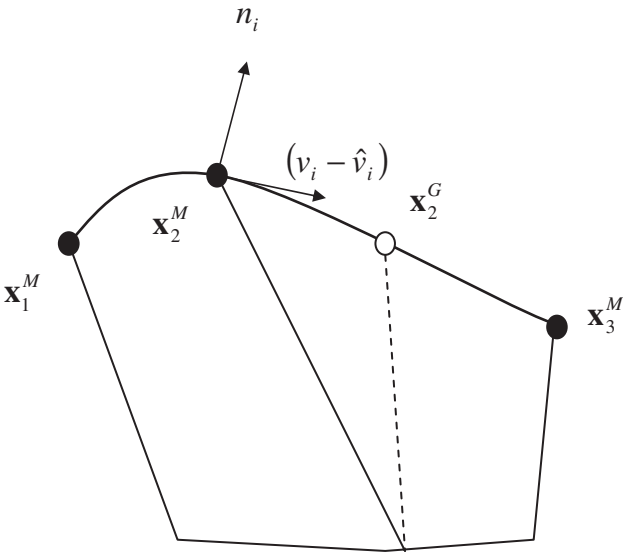

Figure 2. Relocation of a node on boundary.

Setting $Y_i = c_i f$, Equation (27) can be written as

$$\left.\frac{\partial f}{\partial t}\right|_{\chi} + \frac{\partial Y_i}{\partial x_i} = \left.\frac{\partial f}{\partial t}\right|_{X} + f\frac{\partial c_i}{\partial x_i} \tag{41}$$

Applying a weak formulation and Gauss divergence theorem to the Y_i and c_i terms yields

$$\int_{\Omega} \left.\frac{\partial f}{\partial t}\right|_{\chi} \mathrm{d}\Omega = \int_{\Omega} \left.\frac{\partial f}{\partial t}\right|_{X} \mathrm{d}\Omega + \oint_{\Gamma} f c_i n_i \,\mathrm{d}\Gamma - \oint_{\Gamma} Y_i n_i \,\mathrm{d}\Gamma \tag{42}$$

where Ω is the element volume and n_i the outward normal to the element boundary Γ.

By assuming that f and its time derivative are constant within an element, one has

$$\left.\frac{\partial f}{\partial t}\right|_{\chi} = \left.\frac{\partial f}{\partial t}\right|_{X} + \frac{f}{\Omega}\oint_{\Gamma} c_i n_i \,\mathrm{d}\Gamma - \frac{1}{\Omega}\oint_{\Gamma} Y_i n_i \,\mathrm{d}\Gamma \tag{43}$$

Explicit time integration of Equation (43) from time t up to time $t + \Delta t$ gives

$${}^{t+\Delta t} f = f^{\mathrm{L}} + \frac{\Delta t}{2\Omega}\sum_{\Gamma=1}^{n_{\mathrm{e}}} F_{\Gamma}(f^{\mathrm{L}} - f_{\Gamma}^{\mathrm{L}})(1 - \alpha_0 \,\mathrm{sign}(F_{\Gamma})) \tag{44}$$

where f^{L} is the state variable obtained in the updated Lagrangian step, n_{e} the number of boundaries of the element, f_{Γ}^{L} the value of f^{L} at the neighbouring element corresponding to boundary Γ, $F_{\Gamma} = \int_{\Gamma} c_i n_i \,\mathrm{d}\Gamma$, and α_0 represents a parameter that can be chosen in the interval [0, 1]: $\alpha_0 = 0$ represents a centred approximation, whereas $\alpha_0 = 1$ results in a full upwind scheme.

The above derivation is valid for an elementwise constant field. For higher-order fields, each finite element can be divided into various subelements, and each of them can be corresponding to the influence domain of a Gauss point. In this paper, quadrilateral elements with 2×2 integration

DOI: 10.1002/nag

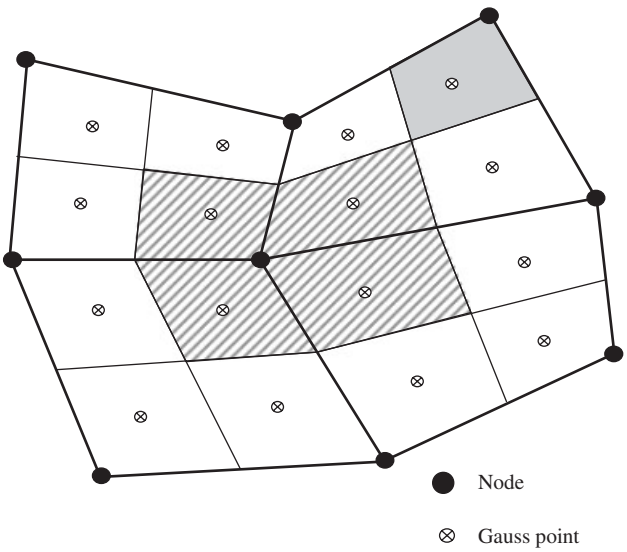

Figure 3. Sub-elements of quadrilateral finite elements.

points are used, and each element is divided into four subelements, as shown in Figure 3. In each subelement, the state variable f is assumed to be constant, and represented by the Gauss-point value. Therefore Equation (44) can be employed to transfer the value of f for each subelement from time t up to time $t + \Delta t$.

For the node centred state variables, the algorithm described above cannot be employed directly. A simple and efficient method is to distribute the values of nodal variables onto the subelements, see Figure 3. These values can be transferred and moved back to the nodes subsequently.

It should be noted that each solution variable includes stress and strain and that the excess pore pressure should be transferred according to the algorithm described above. Because the effective stress-based elasto-plastic constitutive model for saturated soil is adopted, all the non-linear path-dependent material variables associated implicitly with this model should be transferred. Transferring the state variables *via* the Godunov scheme somewhat disrupts equilibrium. It might then be necessary to check the equilibrium and elasticity criteria on the new mesh. However, the UL method is adopted here and the time-step increments are selected to be small enough, and any lack of equilibrium can be overcome after some iteration during the next time step.

4. NUMERICAL EXAMPLES

This section is to examine the efficiency and accuracy of the proposed ALE method in detail using two examples.

4.1. Finite consolidation of a saturated soil column

An analytical solution for the finite consolidation of a homogeneous soil layer was presented by Gibson *et al*. [29] and Monte and Krizek [30]. The solution provides a benchmark for verifying

DOI: 10.1002/nag

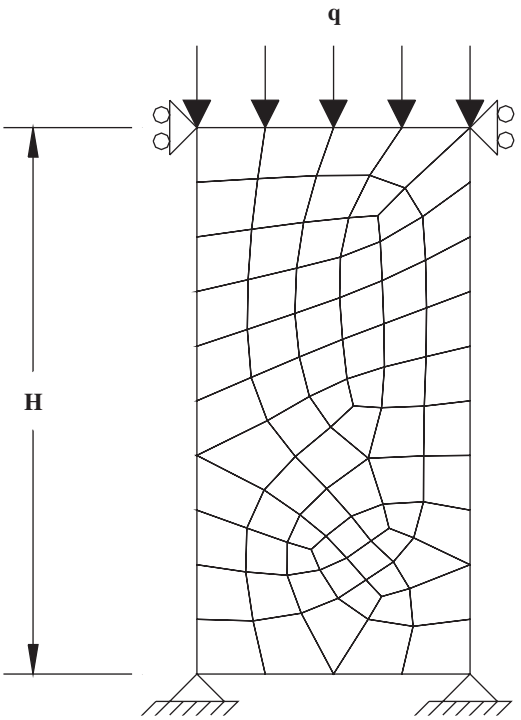

Figure 4. One-dimensional consolidation of a saturated soil column.

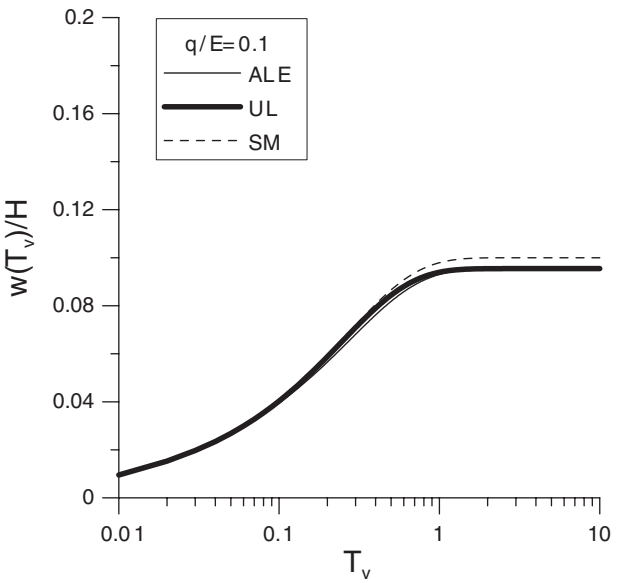

Figure 5. Vertical settlement *versus* normalized time for load level $q = 0.1E$.

DOI: 10.1002/nag

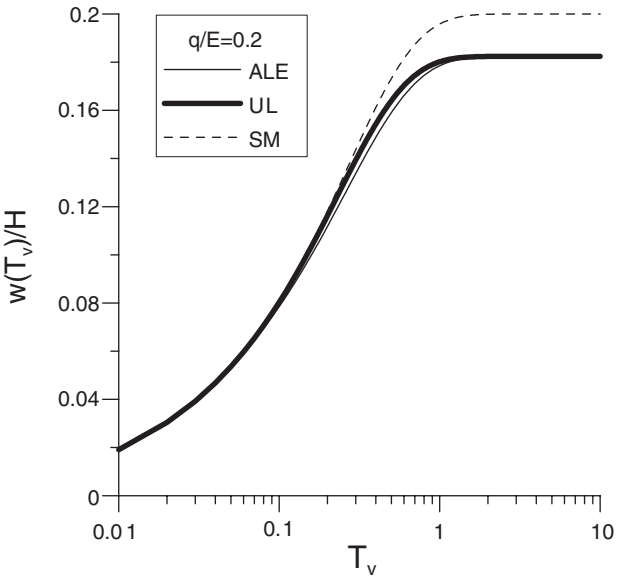

Figure 6. Vertical settlement *versus* normalized time for load level $q = 0.2E$.

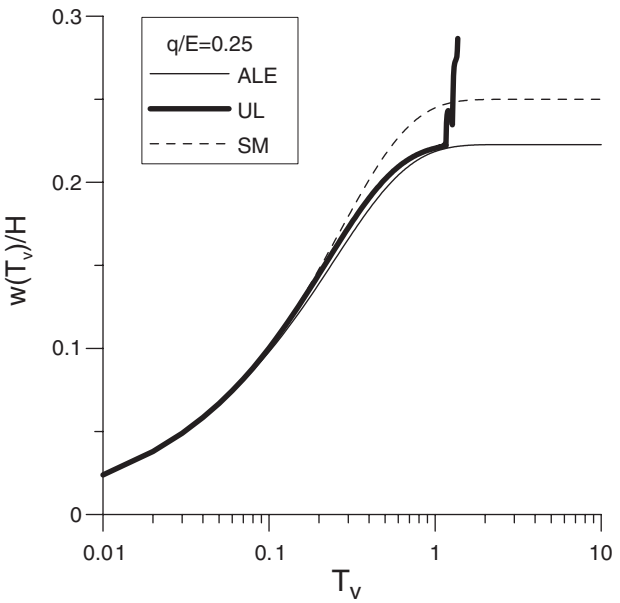

Figure 7. Vertical settlement *versus* normalized time for load level $q = 0.25E$.

DOI: 10.1002/nag

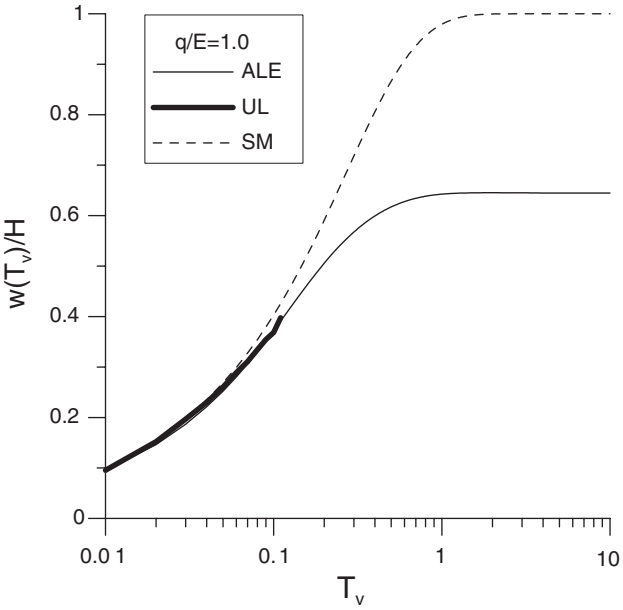

Figure 8. Vertical settlement *versus* normalized time for load level $q = 1.0E$.

the proposed ALE procedure. The discrete model is a one-dimensional problem represented by a saturated soil column under plane strain conditions. The soil is considered elastic with incompressible pore fluid and constant permeability. In order to show the limitation of the UL method and the capability of the proposed ALE method, an irregular mesh shown in Figure 4 is adopted. The nodes at the bottom are fixed in the vertical direction. The lateral boundary of the soil column is assumed as impermeable, and drainage is allowed only through the ground surface. Function q applied at the ground surface is a step load.

To show extreme deformations, the following material parameters which do not necessarily represent a real soil are used: the height $H = 10\,\text{m}$, the elastic modulus of the soils is $E = 100\,\text{MPa}$, the Poisson ratio $v = 0.0$, the soil porosity $n = 0.91$, the permeability $k = 0.01\,\text{m/s}$. Four load levels equalling to 0.1, 0.2, 0.25 and 1.0 times the elastic modulus E are considered. Note that the parameters used here are not for realistic soil.

Figures 5–8 show the vertical settlement at ground surface, W, against the normalized time, $T_\text{V} = C_\text{V} t / H^2$, for different load levels. Here C_V is known as the one-dimensional consolidation coefficient. In the diagrams the thick curves denote the numerical results of the UL method, thin curves denote the numerical results of the proposed ALE method (ALE), and the dashed curves represent the numerical results using the small strain method (SM).

It is noted that the difference between the small and finite strain results increases as the applied load increases and the results of the UL method are close to those of the ALE method at low load levels ($q \leqslant 0.2E$). When the applied load becomes larger, say $q = 0.25E$, some elements are severely distorted at $T_\text{V} = 1.37$ in the updated Lagrangian formulation (Figure 9), leading to instability and termination of the computation. By comparison, when the proposed ALE method

DOI: 10.1002/nag

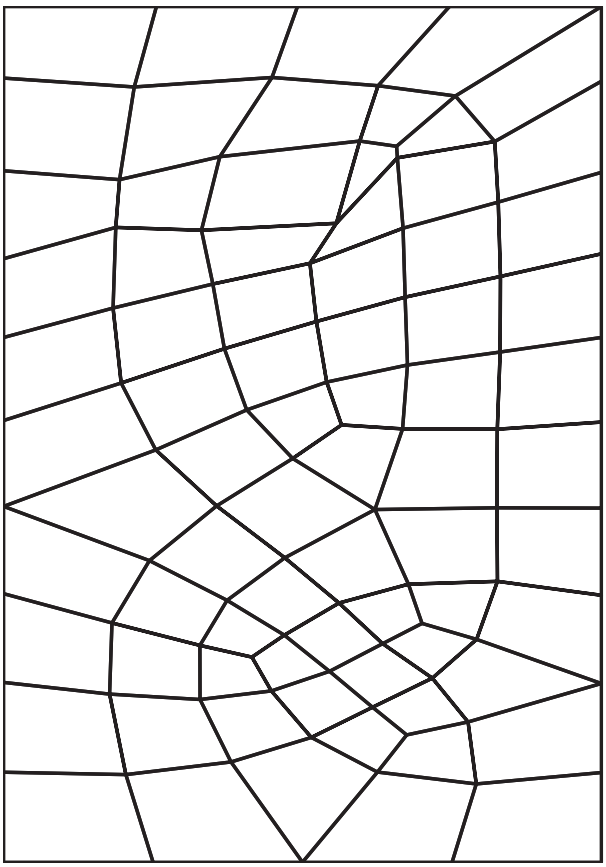

Figure 9. Deformed mesh ($q = 0.25E$) at $T_V = 1.37$ in the updated Lagrangian analysis.

is used, this numerical difficulty is overcome and the computation goes smoothly. The deformed meshes at $T_V = 1.37$ and 10.0 are shown in Figures 10 and 11, respectively.

In the case of load level $q = 1.0E$, the elements are significantly distorted (Figure 12), resulting in the termination of computation at $T_V = 0.10$ in the updated Lagrangian analysis. However, in the proposed ALE analysis the mesh has a good shape as shown in Figure 13. Figure 14 shows the final deformed mesh of the proposed ALE analysis at $T_V = 10.0$.

The theoretical relationships between the applied load, q, and the final vertical settlement, W, derived using the infinite and finite strain theories, and the computed results obtained using the updated Lagrangian and the proposed ALE methods are compared in Figure 15. The theoretical relationship between the applied load and the final settlement for finite strain method is logarithmic, and that for SM linear. The dashed line represents the theoretical solution of small strain (SM), the solid one the theoretical solution of finite strain (FD). The squares are numerical results of SM, the dots are the results of the UL method, and the circles the results computed by the proposed ALE method. Note that for the soil column with the initial configuration shown in Figure 4, *it is*

DOI: 10.1002/nag

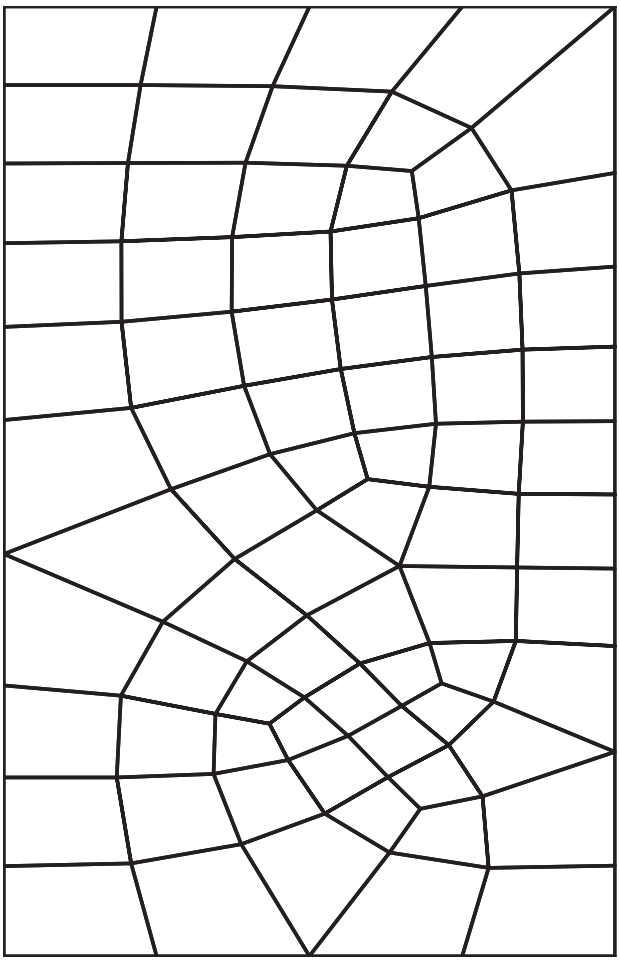

Figure 10. Deformed mesh ($q = 0.25E$) at $T_V = 1.37$ in the proposed ALE analysis.

impossible to correctly obtain the final settlement by using the UL method in cases of the load levels of $q \geqslant 0.25E$. The comparison between the numerical results and analytical solutions in Figure 15 well demonstrates the accuracy and stability of the proposed ALE scheme.

4.2. Seismic response of an embankment

Furthermore, a complex problem of the response of an embankment subjected to vertical and horizontal earthquake motions is analysed here using the proposed ALE scheme. This is a typical plane strain problem, with the initial finite element mesh shown in Figure 16. Infinite elements are used for the lateral boundary sides. The bottom is assumed as impermeable while the ground surface is treated as a drainage boundary. The effective stress based elasto-plastic constitutive model [19] is selected to describe the complicated non-linear behaviour of soils under dynamic loading. Table I gives the model parameters used in the example. More details of the material

DOI: 10.1002/nag

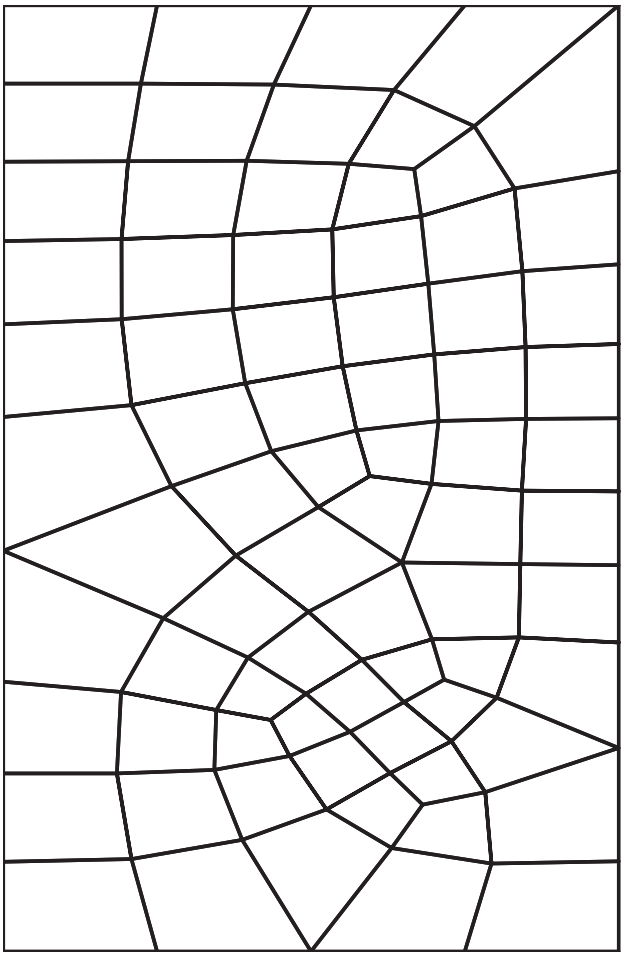

Figure 11. Deformed mesh ($q = 0.25E$) at $T_V = 10.0$ in the proposed ALE analysis.

parameters can be found in [19]. The accelerations recorded at Port Island, Kobe during the 1995 Kobe earthquake (Figure 17) are used as input motions.

In Figure 18 the deformed meshes of the embankment at time 5.1 s by using the updated Lagrangian and proposed ALE methods are compared. There appear some elements whose volumes turn to be negative in the updated Lagrangian analysis (Figure 18(a)), due to severe distortion of the discrete elements. Consequently, computational stability is lost and the running of the program is halted. By comparison, the finite element mesh remains smooth in the ALE formulation (Figure 18(b)) and the computation can be continued. The complete time histories of the horizontal and vertical displacements at point P, predicted using the ALE formulation, are shown in Figure 19, and the time histories of the excess pore pressures at points A, B, C and D are presented in Figure 20. Note that the computed horizontal and vertical displacements at the crest of the embankment are as high as 10 m and 5 m, respectively. Figure 21 shows the deformed configurations and

DOI: 10.1002/nag

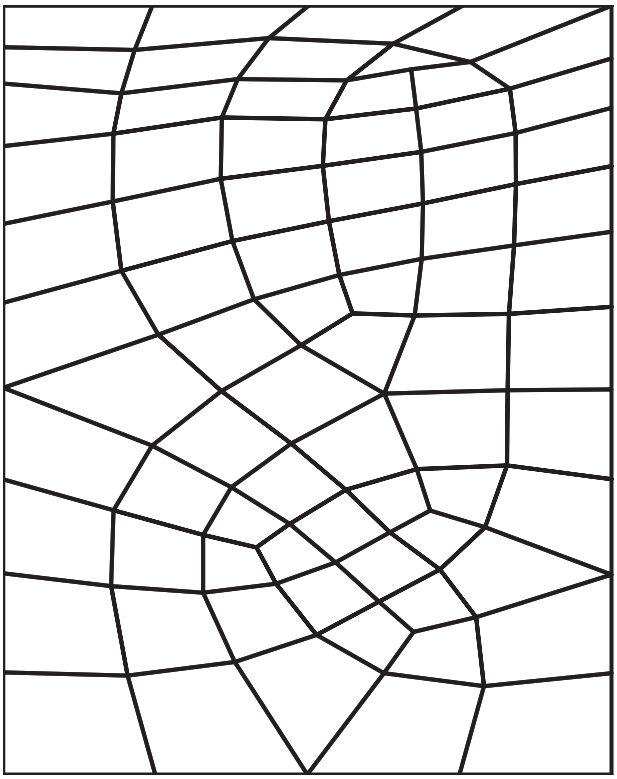

Figure 12. Deformed mesh ($q = 1.0E$) at $T_V = 0.10$ in the updated Lagrangian analysis.

distributions of excess pore pressure ratios (EPPR) at different stages of earthquake motion (i.e. 5.0, 10.0 s and end of the motion). Here, the scale of deformation is the same as that of the finite element mesh and the grey scale varying from black to white represents EPPR from 1.0 to 0.0. It is apparent that the proposed ALE method can provide reasonable predictions for various responses of the embankment during the entire loading history.

5. CONCLUSIONS

Many geotechnical applications such as failure of embankments due to liquefaction and penetration of piles into the ground involve large deformations of geomaterials. Conventional numerical methods based on the infinitesimal strain theory may not be suitable for these applications. How to accurately predict the response of geomaterials at large deformations poses a challenging problem for the geotechnical profession.

This paper has presented an operator-split ALE model for the solution of large deformation problems of saturated soils subjected to static and/or dynamic loading. The solid–fluid coupling and material non-linearity in soils are taken into account. The computation scheme consists of

DOI: 10.1002/nag

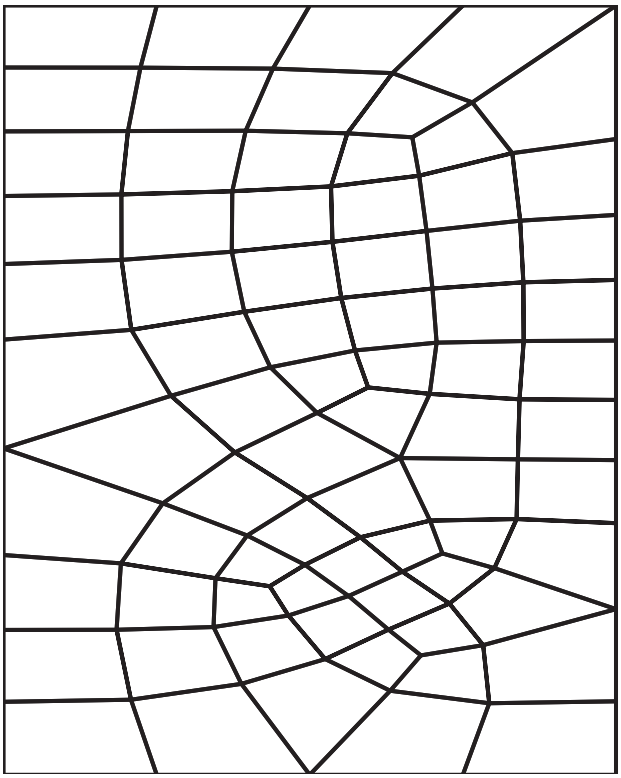

Figure 13. Deformed mesh ($q = 1.0E$) at $T_V = 0.10$ in the proposed ALE analysis.

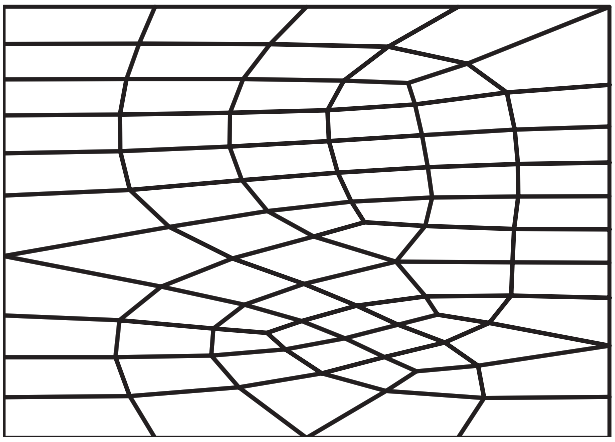

Figure 14. Deformed mesh ($q = 1.0E$) at $T_V = 10.0$ in the proposed ALE analysis.

DOI: 10.1002/nag

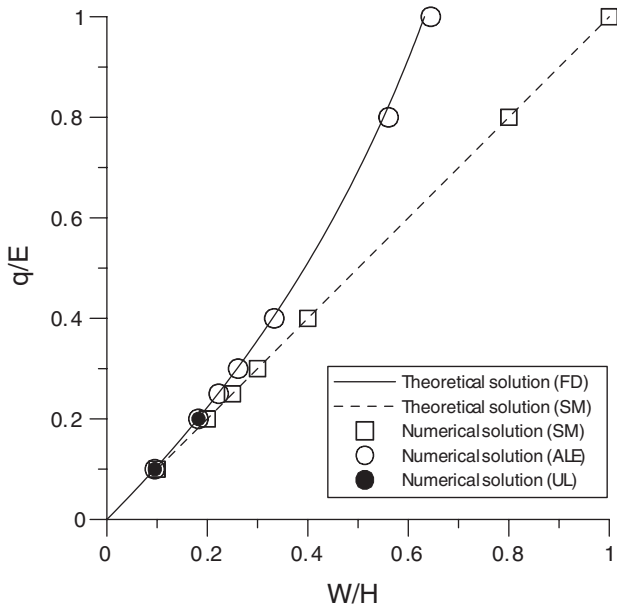

Figure 15. Final vertical settlement *versus* the applied load.

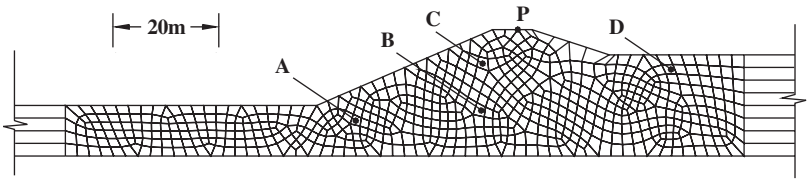

Figure 16. Initial finite element mesh of the embankment.

Table I. Material parameters used for embankment analysis.

Material parameter	Value
Density ρ(t/m)^3	1.830
Coefficient of permeability k(m/s)	4.0E − 6
Initial void ratio e_0	1.10
Compression index λ	0.20
Swelling index κ	0.02
Initial shear modulus ratio G_0/σ'_{m0}	1420.0
Failure stress ratio M_f	1.13
Phase transformation stress ratio M_m	0.71
Hardening parameter B_0	5500.0
Hardening parameter B_1	30.0
Control parameter of anisotropy C_d	2000.0
Dilatancy parameter D_0	1.1
Dilatancy parameter η	3.0

DOI: 10.1002/nag

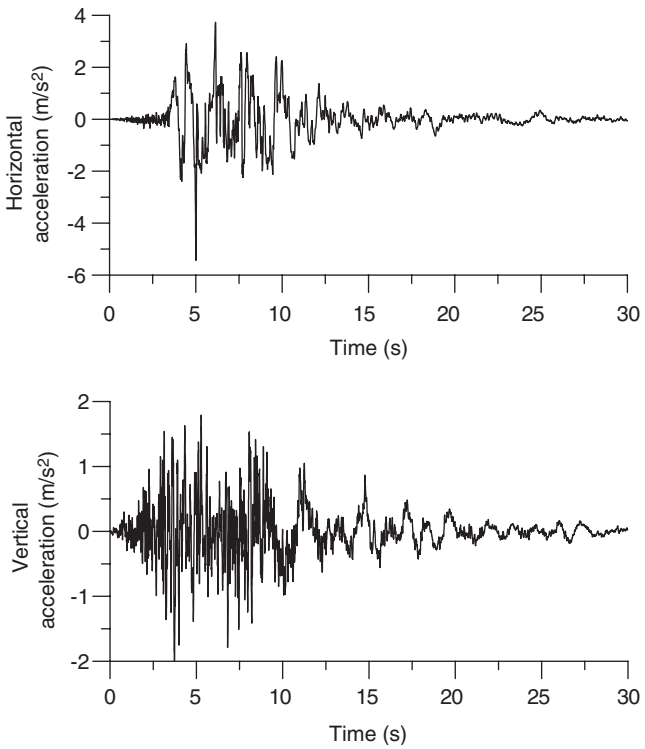

Figure 17. Acceleration records at Port Island, Kobe during the 1995 Kobe earthquake.

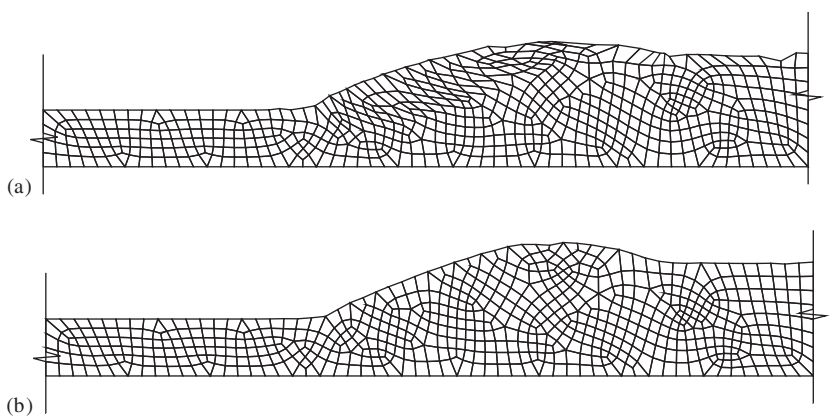

Figure 18. The deformed mesh of the embankment at time 5.1 s: (a) the updated Lagrangian method and (b) the operator-split ALE method.

two steps at each time step: a Lagrangian step and an Eulerian step. In the Lagrangian step, the governing equations of the saturated soil, the equilibrium equation and the continuity equation are solved by the traditional UL method. In the Eulerian step, mesh smoothing and state variables

DOI: 10.1002/nag

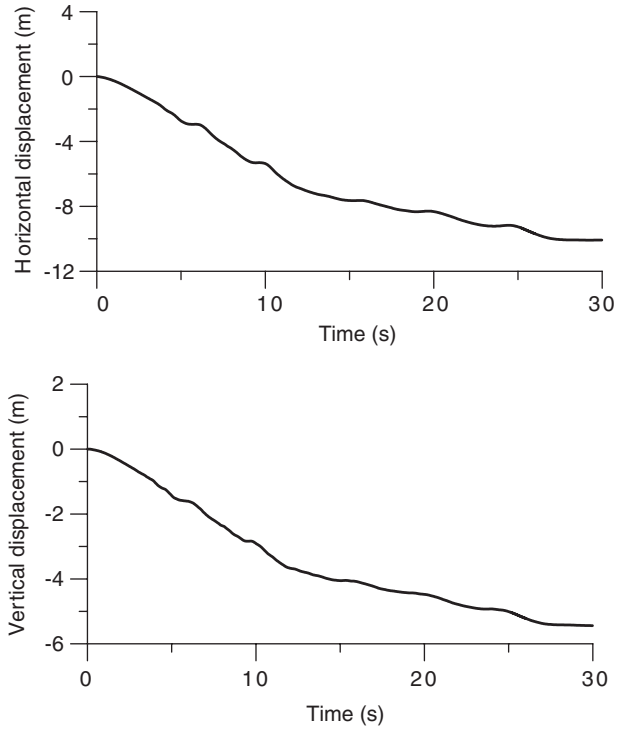

Figure 19. Time histories of the horizontal and vertical displacements at point P.

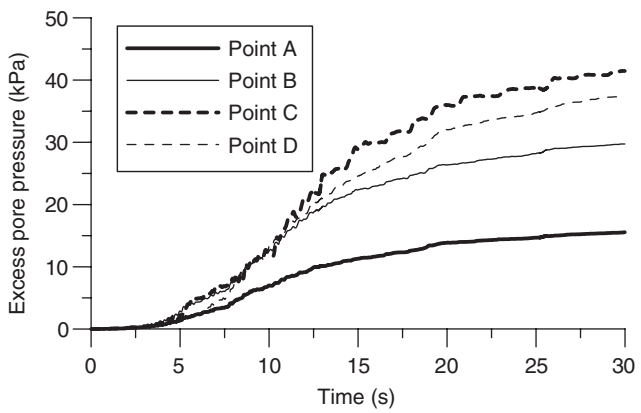

Figure 20. Time histories of excess pore pressure ratios at points A–D.

transferring are performed. An r-adaptivity method that refines the finite element mesh by relocation of nodes is adopted in the mesh-smoothing scheme. The Godunov method is employed to transfer state variables obtained in the updated Lagrangian step to the new mesh system.

DOI: 10.1002/nag

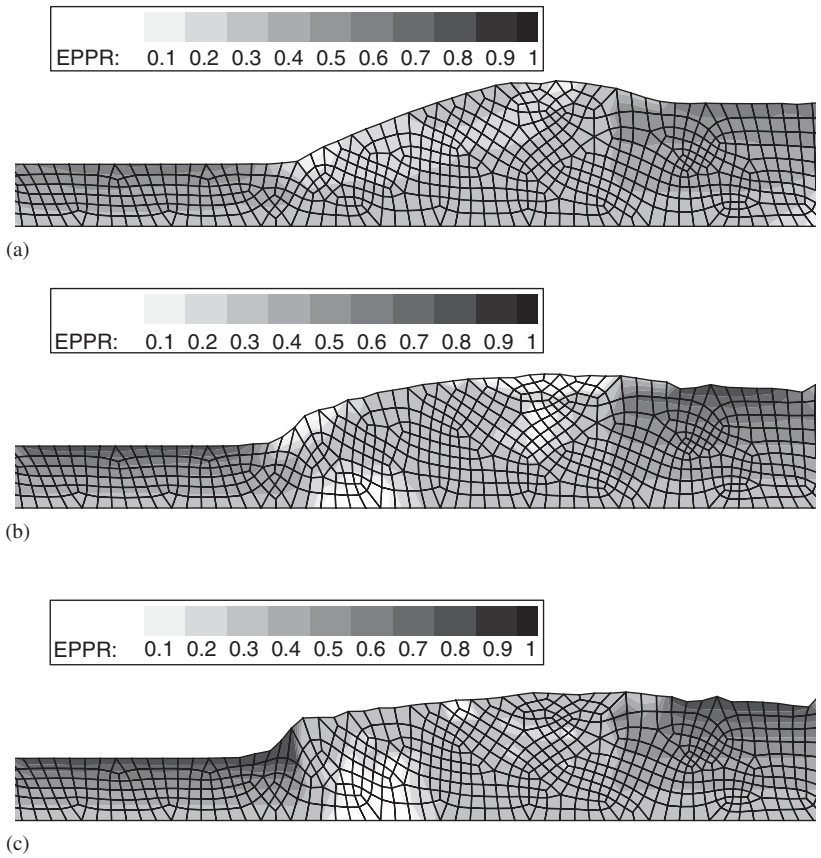

Figure 21. The deformed meshes of the embankment and distributions of excess pore pressure ratios at different stages of earthquake motion: (a) 5.0 s; (b) 10.0 s; and (c) end of the motion.

The performance of the proposed ALE method has been illustrated in detail using examples. The results indicate that the small strain finite element model is not able to provide a good prediction when the deformation of the soil body is significantly large and the updated Lagrangian formulation suffers from numerical instability caused by severe element distortion. It has shown that the proposed ALE method is capable of accounting for the significance of large deformation effects and providing a reasonable simulation even for complex non-linear dynamic problems involving soil liquefaction.

ACKNOWLEDGEMENTS

The financial support provided by the Research Grants Council of Hong Kong (HKU7191/05E) is gratefully acknowledged. The first author would also like to acknowledge the support provided by MEXT of Japan through its 21st Century COE Program at DPRI of Kyoto University.

DOI: 10.1002/nag

REFERENCES

1. Booker JR. A numerical method of solution of Biot's consolidation theory. *Quarterly Journal of Mechanics and Applied Mathematics* 1973; **26**:445–470.
2. Prevost JH. Nonlinear transient phenomena in saturated porous media. *Computer Methods in Applied Mechanics and Engineering* 1982; **20**:3–18.
3. Zienkiewicz OC, Bettess P. Soils and other saturated media under transient, dynamic conditions. *Soils Mechanics Transient and Cyclic Loads*. Wiley: New York, 1982; 1–16.
4. Zienkiewicz OC, Shiomi T. Static and dynamic behaviour of saturated porous medium: the generalized Biot formulation and its numerical solution. *International Journal for Numerical and Analytical Methods in Geomechanics* 1984; **8**:71–96.
5. Zienkiewicz OC. Coupled problems, their numerical solution. In *Numerical Method in Coupled System*, Lewis RW, Bettess P, Hinton E (eds). Wiley: New York, 1984; 35–58.
6. Carter JP, Booker JR, Small JC. The analysis of finite elasto-plastic consolidation. *International Journal for Numerical and Analytical Methods in Geomechanics* 1979; **3**:107–129.
7. Zienkiewicz OC, Chan AHC, Pastor M, Paul DK, Shiomi T. Static and dynamic behaviour of soils: a rational approach to quantitative solutions. I—fully saturated problems. *Proceedings of the Royal Society of London, Series A* 1990; **429**:285–309.
8. Zienkiewicz OC, Xie YM, Schrefler BA, Ledesma A, Bicanic N. Static and dynamic behaviour of soils: a rational approach to quantitative solutions. II—semi-saturated problems. *Proceedings of the Royal Society of London, Series A* 1990; **429**:311–321.
9. Meroi EA, Schrefler BA, Zienkiewicz OC. Large strain static and dynamic semisaturated soil behavior. *International Journal for Numerical and Analytical Methods in Geomechanics* 1995; **19**:81–106.
10. Di Y, Sato T. A practical numerical method for large strain liquefaction analysis of saturated soils. *Soil Dynamics and Earthquake Engineering* 2004; **24**:251–260.
11. Belytschko T, Kennedy JM. Computer models for subassembly simulation. *Nuclear Engineering and Design* 1978; **49**:17–38.
12. Hughes TJR, Liu WK, Zimmermann TK. Lagrangian–Eulerian finite element formulation for incompressible viscous flow. *Computer Methods in Applied Mechanics and Engineering* 1981; **29**:329–349.
13. Haber RB. A mixed Eulerian–Lagrangian displacement model for large deformation analysis in solid mechanics. *Computer Methods in Applied Mechanics and Engineering* 1982; **43**:277–292.
14. Liu WK, Chang H, Chen JS, Belytschko T. Arbitrary Lagrangian–Eulerian Petrov–Galerkin finite element for nonlinear continua. *Computer Methods in Applied Mechanics and Engineering* 1988; **68**:259–310.
15. Ghost S, Kikuchi N. A Lagrangian–Eulerian finite element method for large deformation analysis of elastic-viscoplastic solids. *Computer Methods in Applied Mechanics and Engineering* 1991; **86**:127–188.
16. Gadala MS, Wang J. Formulation and survey of ALE method in nonlinear solid mechanics. *Computer Methods in Applied Mechanics and Engineering* 1998; **167**:33–55.
17. Benson DJ. An efficient, accurate, simple ALE method for nonlinear finite element programs. *Computer Methods in Applied Mechanics and Engineering* 1989; **72**:305–350.
18. Oka F, Yashima A, Shibata T, Kato M, Uzuoka R. FEM–FDM coupled liquefaction analysis of a porous soil using an elastic–plastic model. *Applied Scientific Research* 1994; **52**:209–245.
19. Oka F, Yashima A, Tateishi A, Taguchi Y, Yamashita S. A cyclic elastic–plastic constitutive model for sand considering a plastic-strain dependence of the shear modulus. *Geotechnique* 1999; **49**(5):661–680.
20. Adachi T, Oka F. Constitutive equations for sands and overconsolidated clays and assigned works for sands. *Proceedings of the International Workshop on Constitutive Relations for Soils*, Grenoble, France, 1982; 141–157.
21. Hughes TJR, Winget J. Finite rotation effects in numerical integration of rate constitutive equations arriving in large deformation analysis. *International Journal for Numerical Methods in Engineering* 1980; **15**:1862–1867.
22. Di Y, Sato T. Arbitrary Lagrangian–Eulerian formulation for large deformation analysis of saturated soils. *Proceedings of the 11th International Conference on Soil Dynamics & Earthquake Engineering & the 3rd International Conference on Earthquake Geotechnical Engineering*, Berkeley, U.S.A., 2004; 110–117.
23. Wang J, Gadala MS. Formulation and survey of ALE method in nonlinear solid mechanics. *Finite Element in Analysis and Design* 1997; **24**:253–269.
24. Liu WK, Chen JS, Belytschko T, Zhang YF. Adaptive finite element with particular reference to external work rate on frictional interface. *Computer Methods in Applied Mechanics and Engineering* 1991; **93**:1186–1216.
25. Zavattieri Pablo D, Dari Enzo A, Buscaglia Gustavo C. Optimization strategies in unstructured mesh generation. *International Journal for Numerical Methods in Engineering* 1996; **39**:2055–2071.

DOI: 10.1002/nag

26. Aymone JLF, Bittencourt E, Creus GJ. Simulation of 3D metal-forming using an arbitrary Lagrangian–Eulerian finite element method. *Journal of Materials Processing Technology* 2001; **110**:218–232.
27. Rodriguez-ferran A, Casadei F, Huerta A. ALE stress update for transient and quasistatic processes. *International Journal for Numerical Methods in Engineering* 1998; **43**:241–262.
28. Askes H, Bode L, Sluys LJ. ALE analyses of localization in wave propagation problems. *Mechanics of Cohesive-Frictional Materials* 1998; **3**:105–125.
29. Gibson RE, England GL, Hussey MJL. The theory of one-dimensional soil consolidation of saturated clays: I. Finite nonlinear consolidation of thin homogeneous layers. *Geotechnique* 1967; **17**:261–273.
30. Monte JL, Krizek RJ. One-dimensional mathematical model for large-strain consolidation. *Geotechnique* 1976; **26**(3):495–510.

DOI: 10.1002/nag